iScience

CellPress
OPEN ACCESS

Article

In-cell investigation of the conformational landscape of the GTPase UreG by SDSL-EPR

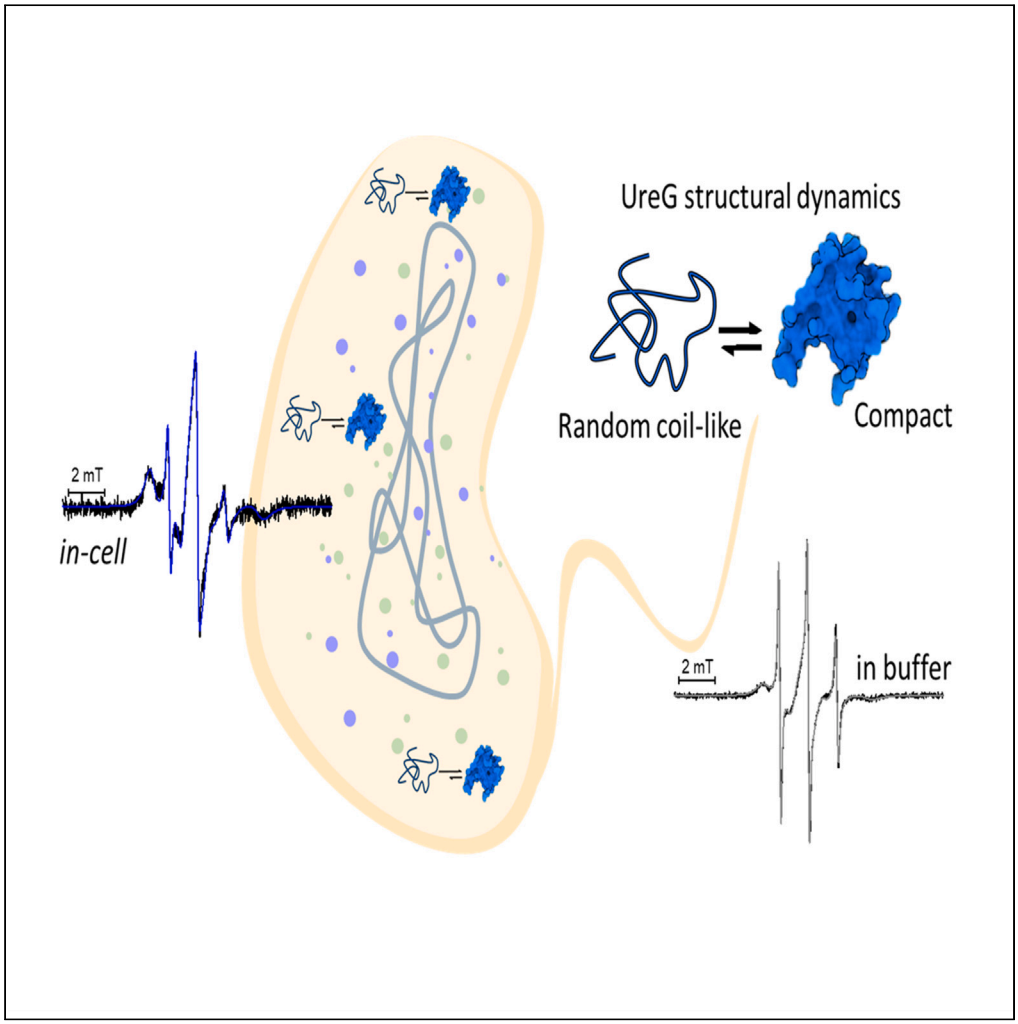

Annalisa Pierro, Ketty Concetta Tamburrini, Hugo Leguenno, ..., Valérie Belle, Barbara Zambelli, Elisabetta Mileo

barbara.zambelli@unibo.it (B.Z.)
emileo@imm.cnrs.fr (E.M.)

Highlights

The conformational landscape of UreG was investigated in bacteria by *in-cell* EPR

In-cell EPR gives access to structural information in a physiological environment

The co-existence of an extended and a compact conformation was found in cell

The structural flexibility of UreG could regulate its enzymatic activity

Pierro et al., iScience *26*, 107855
October 20, 2023
https://doi.org/10.1016/j.isci.2023.107855

iScience

CellPress
OPEN ACCESS

Article

In-cell investigation of the conformational landscape of the GTPase UreG by SDSL-EPR

Annalisa Pierro,[1,2,7] Ketty Concetta Tamburrini,[3,4,7] Hugo Leguenno,[5] Guillaume Gerbaud,[1] Emilien Etienne,[1] Bruno Guigliarelli,[1] Valérie Belle,[1] Barbara Zambelli,[6,*] and Elisabetta Mileo[1,8,*]

SUMMARY

UreG is a cytosolic GTPase involved in the maturation network of urease, an Ni-containing bacterial enzyme. Previous investigations *in vitro* showed that UreG features a flexible tertiary organization, making this protein the first enzyme discovered to be intrinsically disordered. To determine whether this heterogeneous behavior is maintained in the protein natural environment, UreG structural dynamics was investigated directly in intact bacteria by *in-cell* EPR. This approach, based on site-directed spin labeling coupled to electron paramagnetic resonance (SDSL-EPR) spectroscopy, enables the study of proteins in their native environment. The results show that UreG maintains heterogeneous structural landscape *in-cell*, existing in a conformational ensemble of two major conformers, showing either random coil-like or compact properties. These data support the physiological relevance of the intrinsically disordered nature of UreG and indicates a role of protein flexibility for this specific enzyme, possibly related to the regulation of promiscuous protein interactions for metal ion delivery.

INTRODUCTION

Molecular chaperones are essential players for cellular life because they regulate protein folding, interaction, activity, and degradation, all functions that guarantee protein homeostasis. From a structural point of view, their activity implies a sequence of transient, reversible, and promiscuous protein-protein interactions, which are often promoted by fold flexibility. The chaperone UreG assists the activation of urease, a nickel-dependent enzyme produced by bacteria, archaea, fungi, and plants, with important applications for health and agriculture.[1] UreG couples the role as molecular chaperone with an enzymatic role as a GTPase. In ureolytic bacteria, it generally collaborates with three other urease-chaperones (UreF, UreD, and UreE) and couples the energy derived from the GTP hydrolysis to Ni(II) transfer from the metallochaperone UreE toward the platform constituted by UreF and UreD, which eventually delivers Ni(II) to the active site of urease containing a lysine carbamylated in this process.[2]

Crystallographic structures of UreG, in the $UreD_2$-$UreF_2$-$UreG_2$*GDP complex (PBD: 4HI0) from *Helicobacter pylori*[3] and in the $UreG_2$*GMPPNP-Ni(II) (guanylyl imidodiphosphate, a non-hydrolyzable GTP analogue) complex (PBD: 5XKT) from *Klebsiella pneumoniae*,[4] show UreG in a dimeric well-folded structure. Differently, *in vitro* studies, including circular dichroism, intrinsic fluorescence, differential scanning calorimetry, NMR, and native mass spectrometry, revealed that in solution the protein behaves as an ensemble of heterogeneous conformations, featuring different degrees of secondary and tertiary organization.[5–9] The structural flexibility observed for UreG made this protein the first enzyme discovered to be intrinsically disordered (ID) under native conditions.[10,11] Previously, we applied site-directed spin labeling coupled to electron paramagnetic resonance spectroscopy (SDSL-EPR) to study local dynamics of UreG (from *Sporosarcina pasteurii*, *Sp*UreG, and *Helicobacter pylori*, *Hp*UreG) in diluted solution.[12,13] SDSL-EPR investigations are based on the insertion of paramagnetic moieties (e.g., nitroxides, metal-based tags, and trityls) in a specific position of a biomolecule.[14–18] For proteins, cysteine residues are usually employed for label grafting, but tyrosine residues can also be targeted.[19–21] When nitroxide labels are used, the labeled protein can be studied by different EPR approaches, such as continuous-wave EPR (CW-EPR) and double electron-electron resonance (DEER).[22,23] The major asset of CW-EPR experiments is that the EPR spectral shape of nitroxides is highly related to their mobility; this provides information about protein local dynamics, which can be studied in solution and at room temperature. DEER experiments allow to measure distance distributions

[1]Aix Marseille Univ, CNRS, BIP, IMM, 13009 Marseille, France
[2]Department of Chemistry, University of Konstanz, Universitätsstraße 10, 78457 Konstanz, Germany
[3]Aix Marseille Univ, CNRS, AFMB, 13009 Marseille, France
[4]INRAE, Aix Marseille Univ, BBF, 13009 Marseille, France
[5]Aix Marseille Univ, CNRS, IMM, Microscopy Core Facility, 13009 Marseille, France
[6]Laboratory of Bioinorganic Chemistry, Department of Pharmacy and Biotechnology, University of Bologna, 40127 Bologna, Italy
[7]These authors contributed equally
[8]Lead contact
*Correspondence: barbara.zambelli@unibo.it (B.Z.), emileo@imm.cnrs.fr (E.M.)
https://doi.org/10.1016/j.isci.2023.107855

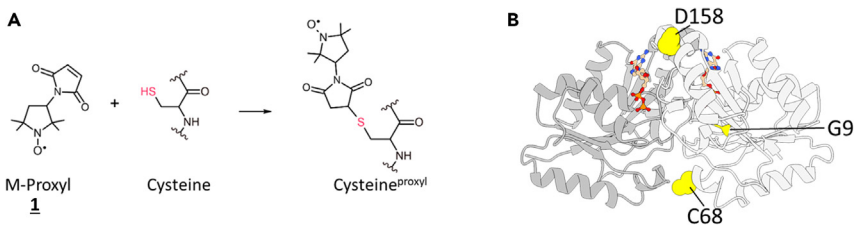

Figure 1. Site-directed spin labeling of *Sp*UreG

(A) Spin-labeling reaction involving M-Proxyl (1) and a cysteine residue.

(B) Model structure of *Sp*UreG obtained by homology modeling from *Hp*UreG crystal structure[3]: the residues targeted for spin labeling are indicated by yellow spheres on one monomer. See also Figure S1.

between two spin labels in the range of 2–8 nm, and the experiments are carried out in frozen solution because of the fast-relaxing properties of spin labels. The SDSL-EPR study of *Sp*UreG and *Hp*UreG revealed that compact and extended conformers are in equilibrium in solution, their presence being modulated by nickel ions or GTP-like substrates[12,13] and that UreG exists in a concentration-dependent monomer/dimer equilibrium, which does not affect its intrinsically disordered state in solution.[12] The well-folded structure found in the crystal state contrasts with the natively flexible state observed in solution, which suggests that the protein acquires a rigid structure only upon binding of its partners. To demonstrate whether this latter behavior is maintained in the natural setting, the conformational state of the protein inside the bacterial cells must be investigated.

The present work unravels the fold and dynamics of *Sp*UreG directly in the interior of bacterial cells, by *in-cell* SDSL-EPR. This technique is a recent approach enabling the study of protein structural dynamics directly inside cells.[14,24,25,26–31] The use of nitroxide-based spin labels allowed running EPR analysis at room temperature, at conditions compatible with the life of the cells under investigation.[32] To study proteins in their native environment, different alternatives are currently available: the spin-labeled protein can be delivered or synthetized directly inside cells,[33–38] and the impact of the cellular environment can be studied by EPR spectroscopy in cells maintained in suspension in a hydrogel and at room temperature.[39] Most of the protocols available to deliver spin-labeled proteins inside cells employs a finely tuned electroporation method.[34,39–41] Here, *Sp*UreG delivery was achieved by modifying a protocol based on the thermal treatment of bacterial cells recently published,[37] which enabled to strongly improve *Sp*UreG intracellular delivery. The results show that *Sp*UreG maintains structural flexibility and heterogeneous landscape *in-cell*, existing in a conformational ensemble of two major conformers, showing either extended or compact properties, both *in-cell* and in solution. Notably, the cellular environment mostly affects the compact conformation, decreasing its mobility and improving its rigidity, whereas the random coil-like conformation remains almost unaffected. The obtained data support the physiological relevance of the ID nature of the GTPase *Sp*UreG.

RESULTS AND DISCUSSION

SpUreG structural dynamics investigated *in vitro* by EPR spectroscopy

To study *Sp*UreG by SDSL-EPR, we prepared several Cys-variants that were conjugated with a paramagnetic spin label selective for thiol groups, the maleimido-proxyl nitroxide (1) (here named "M-Proxyl", Figure 1A). *Sp*UreG (Figure 1B) presents one native cysteine (Cys68) available for labeling, in the Cys-Pro-His metal-binding site,[12] making the wild-type protein useful for grafting spin label 1 (C68^{proxyl}) and monitoring this region of the protein. Other two variants introduced a Cys for labeling in the proximity of the N-terminus P-Loop (Gly-Ser-Gly-Lys-Thr) GTP-binding motif (G9C^{proxyl}) or in the C-terminus of the protein (D158C^{proxyl}), which is involved in the interaction with the chaperone partner UreE.[3] In the latter two variants, Cys68 was mutated in alanine (Cys68Ala) to selectively label only a single position of the protein.[5,42] A double cysteine variant (G9C^{proxyl}/D158C^{proxyl}) served to probe distance distributions between the two spin centers by DEER experiments. The labeling efficiency was over 90% for all variants as confirmed by comparing the double integration of the EPR spectra with the protein concentration and confirmed by mass spectrometry (Figure S1).

EPR spectra of *Sp*UreG variants G9C^{proxyl}, C68^{proxyl}, and D158C^{proxyl} (Figures 2A–2C) showed multicomponent spectra, suggesting that at least two different spectral components coexist. The simulation of experimental data[43,44] (Figures 2M–2O), indicated that all variants present a *sharp* component and a *broad* component of the spectrum: the *sharp* component is characterized by a rotation correlation time (τ_c) $\tau_c \leq 1$ *ns*, typical of unstructured regions.[33,45] The *broad* component is characterized by a higher correlation time that differs between the three variants: in particular, the τ_c of the broad component is significantly lower for C68^{proxyl} (4.0 ns) than for the other two variants (6.5 ns for D158C^{proxyl}; 7.5 ns for G9C^{proxyl}).[12] Although the *broad* and *sharp* components are equally represented for the C68^{proxyl}, both G9C^{proxyl} and D158C^{proxyl} show a prevalence of the broad component (Figures 2M–2O). These results reflect the co-existence of multiple protein substates, initially revealed by the large line broadening of NMR spectra of UreG from multiple sources, the latter indicative of conformational equilibria in the intermediate exchange regime that, for NMR, is typically in the millisecond to microsecond timescale[5,7,9,10,46]; this was subsequently confirmed by native mass spectrometry[8] and SDSL-EPR,[12,13] which also found that several osmolytes perturb protein folding.[12] In this work, the effect of PEG and sucrose on the spectral shape of all the variants was demonstrated (Figures 2 and S7).[47–49]

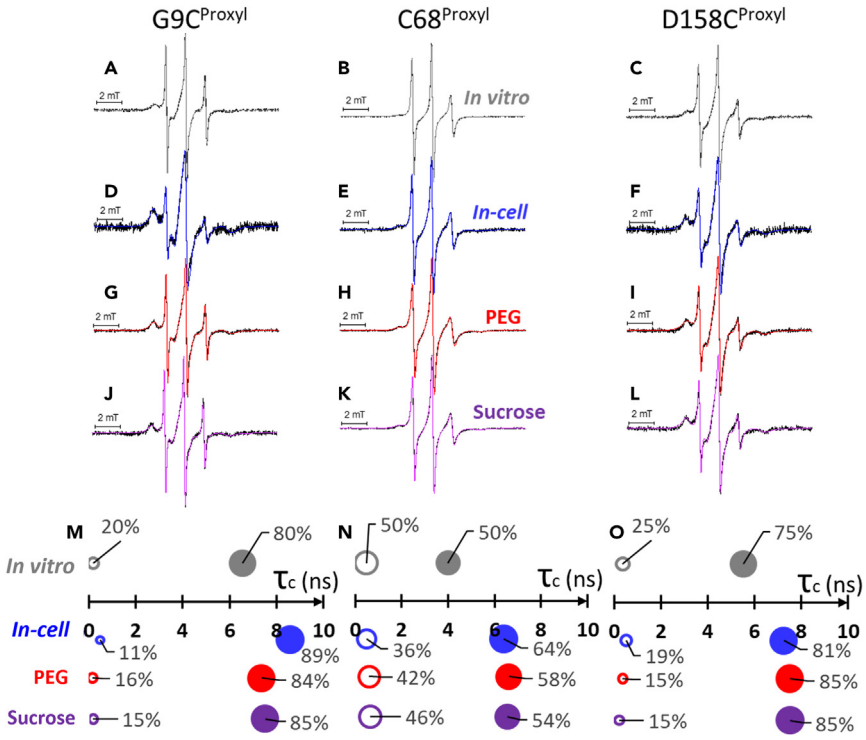

Figure 2. EPR spectra and simulation results

Room temperature, X-band CW-EPR spectra recorded for the studied *Sp*UreG variants labeled with M-Proxyl (1) *in vitro* (single scan in 1.5 min in Tris Buffer 10 mM, pH 7.4, panels A, B, C) and in *E. coli* cells (10 scans in 15 min for panel D, single scan in 1.5 min for panels E and F). RT, X-band CW-EPR spectra of *Sp*UreG variants in presence of PEG8000 200 mg/mL are reported in panel G, H, I; those in Sucrose 20% v/v in panels J, K, L. Experimental data are in black, whereas simulated ones are indicated by colored lines. Scale bars represent 2 mT. Panels M, N, and O summarize simulation results: τ_c extracted from the simulations are plotted on the x axis; the percentage of each population described by a τ_c is represented as a surface of a sphere. The IDP-sharp component is reported in empty spheres, the broad-compact one as filled sphere. Simulation results of EPR spectra in the presence of crowding agents are colored as follows: blue for *in-cell* data; red for PEG8000 200 mg/mL; purple for Sucrose 20% v/v. See also Figures S2, S3, S6, S8, and S12 and Table S1.

Concerning the two protein substates, one is more compact and mostly found in the proximity of the protein core and of the GTP-binding region and the other disordered and more abundant in the surrounding of the metal-binding domain.

SpUreG local dynamics in cellular context

Delivery of spin-labeled UreG into E. coli cells

In-cell EPR experiments are conducted by prior labeling of the protein of interest, produced by recombinant expression, and by delivering it inside cells.[24,41] Recently, we investigated the structural dynamics of the bacterial protein NarJ in its native environment, *E. coli* cells. The delivery of labeled NarJ into bacteria was achieved by electroporation.[39] Here an alternative and recently reported delivery protocol, based on thermal shock,[37,38] was adapted for the delivery of *Sp*UreG and compared with electroporation. In particular, Ca(II) ions, in combination with a short incubation at 42°C, were used to trigger protein delivery (Figure S2). Ca(II) ions are necessary for protein internalization: in the absence of Ca(II) no internalization can be detected (Figure S3).

Ca(II) is a known precipitating agent; its concentration should be carefully evaluated. The set-up of this parameter was done using the super-folded (*sf*)GFP as a model system, and the internalization of the protein was followed by fluorescence microscopy (Figure 3 andS4). Addition of 50 mM $CaCl_2$ caused protein aggregation around the bacteria (Figure 3A); differently, in the presence of 10 mM $CaCl_2$, the protein was properly internalized and no aggregates are visible (Figure 3B). Coherently, the average fluorescence, measured for each bacterium, normalized to the background of the image (Figure S5) shows that bacteria acquire significantly more GFP when they are treated with 10mM $CaCl_2$ than with 50 mM, because the aggregates outside the cells decrease the signal-to-noise ratio. The nonspecific interaction of the protein with the cell membrane was excluded by the absence of fluorescence for a sample not subjected to the thermal treatment in the presence of 10 mM $CaCl_2$ (Figure 3C, S4, and S6). Cell viability was not affected by the presence of 10 mM $CaCl_2$ (Figure S7). Therefore, 10 mM of Ca(II) was chosen as optimal concentration to exogenously deliver *Sp*UreG by thermal shock into cells.

EPR spectra obtained by delivering all the *Sp*UreG variants into *E. coli* cells by electroporation (Figures 4A–4C) and thermal shock (Figures 4D–4F), applied to the same number of cells (4–7 x 10^{10} cells/mL), show that the former protocol is not efficient and that the amount

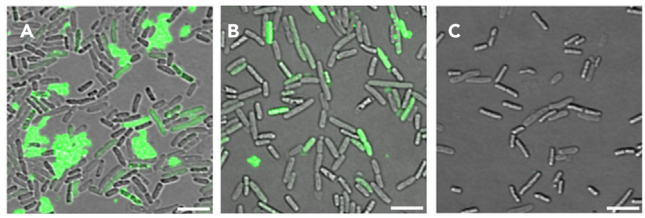

Figure 3. *sf*GFP internalization in *E. coli* cells followed by fluorescence microscopy

(A–C) Transmission (DIC) and fluorescence (MIP) image overlays of *E. coli* cells in which sfGFP was delivered by heat-shock in the presence of 50 mM (A) and 10 mM (B) Ca(II). Control experiments (C) were performed by analyzing bacteria incubated with *sf*GFP without performing the heat-shock. Scale bars represent 2 μm. See also Figures S4–S7.

of *Sp*UreG delivered into cells was insufficient to provide good EPR signal-to-noise ratio. Differently, thermal shock provided ~20-fold higher EPR signal-to-noise ratio and sensibly reduced the acquisition time window from 50 min to 1–15 min, according to the spectral shape obtained.

Reducing the acquisition time is important to preserve the viability of the bacteria under investigation and limit the decrease of intracellular nitroxide signal over time, due to its cytosolic reduction to hydroxylamine, a silent EPR derivative.[24,50] No significant changes of EPR spectral shapes of the *Sp*UreG variants delivered by heat-shock or electroporation were observed, indicating that the *in-cell* EPR data depend on the cellular environment and not on the delivery method. All these considerations prompted us to use the thermal shock protocol for the preparation of all *in-cell* samples. This comparative analysis points out the importance of individually optimizing the delivery methods for different exogenous protein into the cells.

Local structural dynamics of SpUreG in the cellular context

The EPR spectra of all *Sp*UreG variants delivered into the bacterial cells (Figures 2D–2F) are characterized by a general broadening of line shapes as compared with the *in vitro* samples (Figures 2A–2C), indicating a decrease of nitroxide *mobility*. Quantitative simulations of the spectra (Figures 2M–2O) indicated that the protein landscape maintains its heterogeneity in the bacterial cytoplasm and can be dissected into two different conformations, represented by a *sharp* and a *broad* component, as reported *in vitro*. A component-dependent response to the cellular environment was observed: the τ_c of the *broad* component increases of ca. 1.5 times, reaching values close to what was expected for well-folded and rigid protein regions; differently, the sharp component maintains very low values of τ_c typical of disordered regions (Table S1). The relative amount between the *sharp* and *broad* components slightly shifts toward the *broad* one in all the labeled positions, indicating an increased ratio of the most compact conformations.

Overall, position C68 is the one characterized by the higher fraction of fast-dynamics component, whereas the other two positions, G9C and D158C, are characterized by a lower fraction, with a trend that is similar to the one found in solution. This conformational response to the cellular environment is remarkably different from the one we previously observed for NarJ, another flexible chaperone with a similar molecular

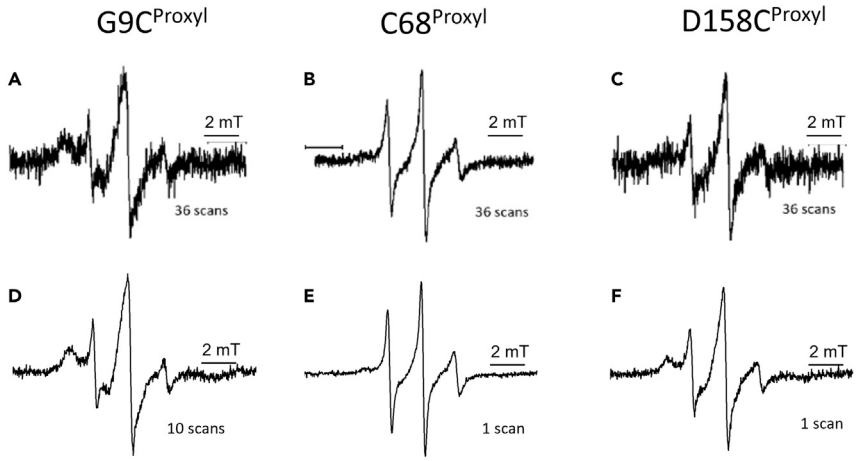

Figure 4. Comparison of EPR spectra of UreG variants delivered into *E. coli* cells by electroporation or heat-shock

Room temperature, X band, CW-EPR spectra of *Sp*UreG variants delivered in *E. coli* cells by electroporation (A, B, C) or heat-shock (D, E, F), respectively. Panels A and D: *Sp*UreG-G9C^{Proxyl}; panels B and E: *Sp*UreG-C68^{Proxyl}; panels C and F: *Sp*UreG-D158C^{Proxyl}. The number of scans recorded for each spectrum is indicated for each of them (36 scans for electroporation—50 min of acquisition, 1–10 for heat-shock, 1–15 min of acquisition. Scale bars represent 2 mT.

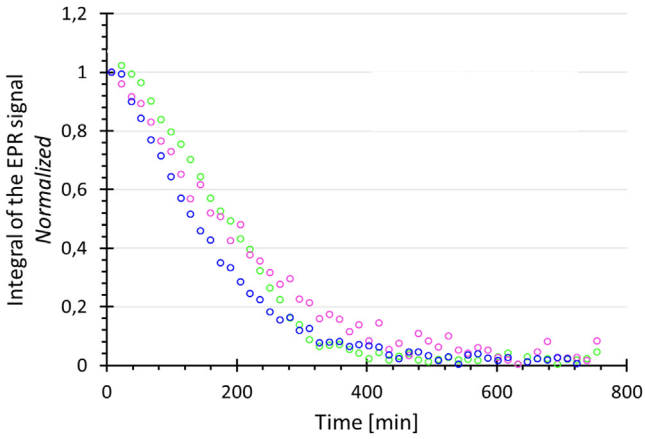

Figure 5. Nitroxide reduction profiles in the cytosol of *E. coli* cells

Normalized integrated intensity of the EPR spectra of all nitroxide-labeled *Sp*UreG variants in *E. coli* over time: C68^{proxyl} in blue, G9C^{proxyl} in magenta, and D158C^{proxyl} in green. Each point represents the normalized double integral of the sum of 10 consecutive EPR spectra.

weight, whose structural dynamics was affected strongly and in a site-specific way by the cytosolic environment, with τ_c variations strictly related to the investigated region.

The conformational response of *Sp*UreG to the cellular environment was further investigated, analyzing the behavior of structural dynamics in highly concentrated crowder solutions containing polymers, sugars, and osmolytes often used to mimic, *in vitro*, cellular confinement, nonspecific interactions, and charge-charge repulsion that proteins experience in the cytoplasm.[51,52] In particular, we tested (1) two synthetic polymers, polyethylene glycol (PEG) and Ficoll, that behave like semi-rigid spheres, thus mimicking globular macromolecules;[53,54] (2) their corresponding monomers, sucrose and ethylene glycol, respectively[52]; and (3) bovine serum albumin (BSA), which mimics nonspecific protein-protein interactions.[55] These molecules only slightly affected the spectral features of *Sp*UreG variants (Figure S8A) with the exception of PEG8000 and sucrose (Figure 2). Results of quantitative simulation of the spectra (Figure S8B) indicated that, as the cellular environment, the crowding agents mostly impacted on the dynamics of the *broad* component, with τc shifting toward higher values, whereas the *sharp* component was only slightly affected. In the case of "protecting agents," such as PEG, Ficoll, and sucrose, this result is not surprising because they have already been shown to stabilize protein folding by lowering the energy of the least hydrated conformer.[56,57]

PEG8000 and sucrose induced spectral changes very similar to those observed *in-cell*, with the correlation time of the broad component increasing by 2 ns for C68^{proxyl} and D158C^{proxyl} and 1 ns for G9C^{proxyl}. Differently, Ficoll and EthG promoted an increase of the relative amount of the *broad* component in G9C^{proxyl} and induced only a mild effect on the other two variants. BSA affected only the D158C^{proxyl} variant, promoting a slight stabilization of the broad component.

Nitroxide reduction in the cytosol during time

In the cytosol, nitroxides are reduced to the corresponding EPR silent hydroxylamine under the action of enzymes and antioxidants, such as glutathione.[24,50] Reduction rates of nitroxide labels, obtained by following the intensity of the EPR signal inside cells upon time, are proportional to the accessibility of the site to which the nitroxide is grafted. The more the nitroxide is reduced, the more the site results to be accessible to the reductants. For example, in our previous study on NarJ chaperone, it undergoes important structural changes *in-cell* that affect the reduction rate of the grafted nitroxide, in a site-dependent way, with the most buried sites being those showing the slower reduction.[39] For *Sp*UreG, all variants are reduced at the same rate *in-cell* (Figure 5), indicating that the accessibility of the reducing agent is similar for all the labeled positions and clearly supporting a diffuse structural flexibility of *Sp*UreG tertiary structure in the cytosol.

SpUreG conformational ensemble by DEER-EPR

Distances between different protein regions were obtained applying DEER-EPR on the doubly labeled *Sp*UreG G9C^{proxyl}/D158C^{proxyl} *in vitro* and in *E. coli* cells. *In vitro*, the absence of oscillation in the time trace (Figures S9A and S9B) results in a large distance distribution (Figure S9C) that spans a broader range than those predicted by MMM calculation,[58] from the available *Hp*UreG crystal structure (Figure S9C, *green area*). In the case of distance distributions characterized by a full width at half maximum (FWHM) larger than 20 Å,[59] this indicates high protein flexibility and in our case that the two labels attached to the protein are not on rigid positions but move one respect to the other along the tertiary structure, supporting the existence of a conformational ensemble in solution.

Concerning *in-cell* experiments, the sample was prepared by delivering the doubly labeled variant inside *E. coli* cells via the heat-shock protocol described before. Approximatively ~15 min after the thermal shock, the sample was shock-frozen in liquid nitrogen to perform DEER experiments at 60 K. *In-cell* DEER traces presented a good signal-to-noise ratio and modulation depth in the cellular environment (Figure 6A), but the reliability distance distributions were compromised by the short-phase memory relaxation time (T_m), which was 0.3 μs in cell versus

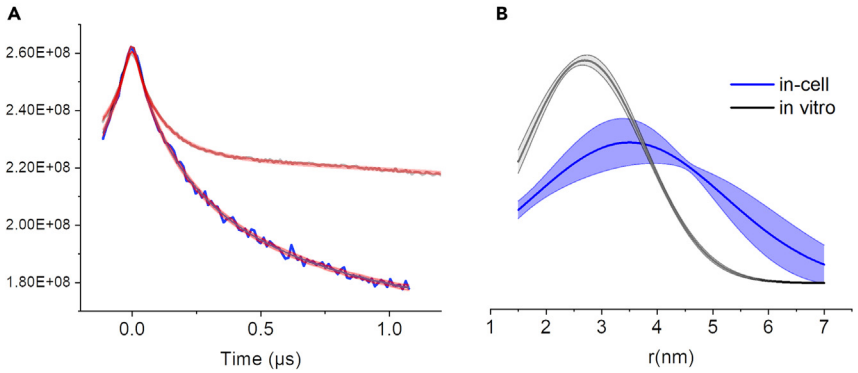

Figure 6. DEER data obtained for *Sp*UreG-G9C^{proxyl}/D158C^{proxyl} in buffer (black traces) and *in-cell* (blue traces)

(A and B) Results of the DEER raw data fitting using DEERLab with a single Gaussian model.[62] The resulting distances are reported in panel B (shaded gray and blue areas represent the uncertainty). The raw time traces and the comparison of the distance distributions extracted using different models are reported in S10. See also Figures S9 and S11.

3 μs, measured in solution (Figure S10A). Short T_m values in the cellular context have already been observed for other proteins.[60,61] An evaluation of the form factor of the raw data and the shape of distance distribution, as well as a comparison with the *in vitro* data (Figure 6B), indicated that the protein maintains a high flexibility of its tertiary structure in cell.

The fact that in this work the CW-EPR study on cells reveals that UreG gains structure is not in contradiction with the DEER results, simply because they give information about different structural level of the protein under investigation. The high flexibility in the tertiary structure of UreG is also confirmed by the result of the nitroxide reduction inside cells.

Conclusions

Previous studies demonstrated that, in solution, the GTPase *Sp*UreG populates at least two conformational states: a compact one and a random coil-like one, whose prevalence in solution could be modulated by denaturants or osmolytes.[12] Three singly labeled variants of UreG (C68^{proxyl}, G9C^{proxyl}, D158C^{proxyl}) were used to monitor different regions of the protein tertiary structure. The EPR spectra show that, in solution, different regions of the protein experience a similarly heterogeneous conformational landscape, with the more compact conformation being prevalent around the catalytic core (G9), whereas the metal-binding site (C68) of the protein shows a higher backbone flexibility, similarly to what previously observed for *Hp*UreG.[13]

Is this conformational equilibrium conserved in the physiological environment? To answer this question, we investigated the local and global dynamics of *Sp*UreG in the cytoplasm of *E. coli* cells. The properties of nitroxide labels to sample protein local dynamics by EPR spectroscopy at room temperature and the development of efficient intracellular delivery method for labeled proteins allowed us to observe that both compact and flexible conformations exist in the cellular environment, represented by the *broad* and a *sharp* components of the *in-cell* EPR spectra, similar to those found in solution. The compact conformer is mostly affected by the cellular environment, showing a significant reduction of the protein mobility in all the studied positions. This change in protein dynamics can be attributed either to the acquisition of additional structural elements or to the compaction of the existing structures by tertiary contacts. However, the protein does not acquire a fully compact state *in-cell*: the equal accessibility of reducing agents to the labels bound to different regions of the protein, as well as the broad distance distributions extracted by DEER analysis, demonstrates that the global flexibility of the tertiary structure is maintained in cellular context. The use of crowding agents only partially reproduces the *E. coli* intracellular conditions. The heterogeneity of the conformational landscape of *Sp*UreG, maintained in its physiological environment, suggests a role of protein flexibility for this specific GTPase enzyme, possibly related to the regulation of promiscuous protein interactions for metal ion delivery. At the same time, the decrease of protein dynamics and *in-cell* fold compaction observed mainly in the catalytic region suggests that *Sp*UreG catalytic activity requires structural rigidity to perform its physiological function. *Sp*UreG folding and dynamics are the results of the compromise between two opposite conformational requirements: a prevalence of structural rigidity, needed for the GTPase function, is found in the protein catalytic core (position G9C), whereas backbone flexibility, required for the intrinsic regulation of activity and protein interactions, is distributed along the backbone mostly in the metal-binding (C68) and protein-protein interaction area (D158C).

Limitations of the study

In the present work, we demonstrated that the GTPase UreG presents a heterogeneous conformational landscape not only *in vitro*, as previously reported, but also in the bacterial cytoplasm. Even though the conditions tested can be considered a very good approximation of the physiological environment, some differences remain with the *in-cell* state that could, in principle, influence the protein conformational distribution and activity of UreG. Indeed, *E. coli* and *Sporosarcina pasteurii* intracellular environments can be different, thus the possibility that the conformational behavior of UreG in *S. pasteurii* cytoplasm differs from the one observed in *E. coli* cannot be excluded. In addition,

S. pasteurii expresses other urease chaperones with which UreG interacts and are not expressed in *E. coli*. The presence of cognate proteins might influence the protein conformational state, probably driving it toward the more folded state.

STAR★METHODS

Detailed methods are provided in the online version of this paper and include the following:

- KEY RESSOURCES TABLE
- RESOURCE AVAILABILITY
  - Lead contact
  - Materials availability
  - Data and code availability
- METHODS DETAILS
  - *Sp*UreG purification and spin-labeling
  - *sf*GFP purification
  - Preparation of competent *E. coli* cells for heat-shock
  - Preparation of competent *E. coli* cells for electroporation
  - Protein delivery by heat-shock and electroporation
  - Fluorescence Microscopy
  - Fluorescence microscopy image analysis
  - CW-EPR experiments *in vitro* and in crowded solutions
  - DEER experiments
- QUANTIFICATION AND STATISTICAL ANALYSIS

SUPPLEMENTAL INFORMATION

Supplemental information can be found online at https://doi.org/10.1016/j.isci.2023.107855.

ACKNOWLEDGMENTS

The authors are grateful to the EPR facilities at the French Research Infrastructure INFRANALYTICS (FR2054) and the Aix-Marseille University EPR center. We also acknowledge support from MOSBRI, which has received funding from the European Union's Horizon 2020 Research and Innovation Programme under Grant Agreement N° 101004806. We acknowledge Dr. Deborah Byrne of the Protein Expression facility at the *Institut de Microbiologie de la Mediterranée* (IMM, Marseille, France) for UreG purification. We thank P. Mansuelle and R. Lebrun from Aix-Marseille University and CNRS IMM (FR 3479), Plateforme de Proteomique, 31 chemin Joseph Aiguier, F-13402 Marseille, France, for mass spectrometry measurements and analyses. We acknowledge financial support from the "Agence Nationale de la Recherche" (ANR-18-CE11-0007-01) and from the "Conseil Régional Région Sud" (A.P. PhD Fellowship EJD-2018-2021). The project leading to this publication has received funding from the A*Midex Foundation of Aix-Marseille University, funded by socioeconomic partners.

AUTHOR CONTRIBUTIONS

Conceptualization, B.Z. and E.M.; Methodology, A.P., K.C.T., G.G., E.M., and H.L. Investigation, A.P., K.C.T., G.G., and H.L.; Data curation, A.P., H.L., G.G., and E.E.; Formal analysis, E.E., B.G., V.B., E.M., and B.Z.; Funding acquisition, B.G. and E.M.; Project administration, B.Z. and E.M.; Software, E.E.; Validation, Writing—original draft, A.P., V.B., B.Z., and E.M. All the authors contributed to the final version of this manuscript.

DECLARATION OF INTERESTS

The authors declare no competing interests.

INCLUSION AND DIVERSITY

We support inclusive, diverse, and equitable conduct of research.

Received: April 7, 2023
Revised: July 7, 2023
Accepted: September 6, 2023
Published: September 9, 2023

REFERENCES

1. Maroney, M.J., and Ciurli, S. (2014). Nonredox nickel enzymes. Chem. Rev. *114*, 4206–4228. https://doi.org/10.1021/cr4004488.
2. Zambelli, B., Musiani, F., Benini, S., and Ciurli, S. (2011). Chemistry of Ni2+ in urease: sensing, trafficking, and catalysis. Acc. Chem. Res. *44*, 520–530. https://doi.org/10.1021/ar200041k.
3. Merloni, A., Dobrovolska, O., Zambelli, B., Agostini, F., Bazzani, M., Musiani, F., and Ciurli, S. (2014). Molecular landscape of the interaction between the urease accessory proteins UreE and UreG. Biochim. Biophys. Acta *1844*, 1662–1674. https://doi.org/10.1016/j.bbapap.2014.06.016.
4. Yuen, M.H., Fong, Y.H., Nim, Y.S., Lau, P.H., and Wong, K.-B. (2017). Structural insights into how GTP-dependent conformational changes in a metallochaperone UreG facilitate urease maturation. Proc. Natl. Acad. Sci. USA *114*, E10890–E10898. https://doi.org/10.1073/pnas.1712658114.
5. Zambelli, B., Turano, P., Musiani, F., Neyroz, P., and Ciurli, S. (2009). Zn2+-linked dimerization of UreG from Helicobacter pylori, a chaperone involved in nickel trafficking and urease activation. Proteins *74*, 222–239. https://doi.org/10.1002/prot.22205.
6. Zambelli, B., Cremades, N., Neyroz, P., Turano, P., Uversky, V.N., and Ciurli, S. (2012). Insights in the (un)structural organization of Bacillus pasteurii UreG, an intrinsically disordered GTPase enzyme. Mol. Biosyst. *8*, 220–228. https://doi.org/10.1039/c1mb05227f.
7. Real-Guerra, R., Staniscuaski, F., Zambelli, B., Musiani, F., Ciurli, S., and Carlini, C.R. (2012). Biochemical and structural studies on native and recombinant Glycine max UreG: a detailed characterization of a plant urease accessory protein. Plant Mol. Biol. *78*, 461–475. https://doi.org/10.1007/s11103-012-9878-1.
8. D'Urzo, A., Santambrogio, C., Grandori, R., Ciurli, S., and Zambelli, B. (2014). The conformational response to Zn(II) and Ni(II) binding of Sporosarcina pasteurii UreG, an intrinsically disordered GTPase. J. Biol. Inorg. Chem. *19*, 1341–1354. https://doi.org/10.1007/s00775-014-1191-9.
9. Miraula, M., Ciurli, S., and Zambelli, B. (2015). Intrinsic disorder and metal binding in UreG proteins from Archae hyperthermophiles: GTPase enzymes involved in the activation of Ni(II) dependent urease. J. Biol. Inorg. Chem. *20*, 739–755. https://doi.org/10.1007/s00775-015-1261-7.
10. Zambelli, B., Stola, M., Musiani, F., De Vriendt, K., Samyn, B., Devreese, B., Van Beeumen, J., Turano, P., Dikiy, A., Bryant, D.A., and Ciurli, S. (2005). UreG, a chaperone in the urease assembly process, is an intrinsically unstructured GTPase that specifically binds Zn2+. J. Biol. Chem. *280*, 4684–4695. https://doi.org/10.1074/jbc.M408483200.
11. Zambelli, B., Mazzei, L., and Ciurli, S. (2020). Intrinsic disorder in the nickel-dependent urease network. Prog. Mol. Biol. Transl. Sci. *174*, 307–330. https://doi.org/10.1016/bs.pmbts.2020.05.004.
12. Palombo, M., Bonucci, A., Etienne, E., Ciurli, S., Uversky, V.N., Guigliarelli, B., Belle, V., Mileo, E., and Zambelli, B. (2017). The relationship between folding and activity in UreG, an intrinsically disordered enzyme. Sci. Rep. *7*, 5977. https://doi.org/10.1038/s41598-017-06330-9.
13. Pierro, A., Etienne, E., Gerbaud, G., Guigliarelli, B., Ciurli, S., Belle, V., Zambelli, B., and Mileo, E. (2020). Nickel and GTP Modulate Helicobacter pylori UreG Structural Flexibility. Biomolecules *10*, 1062.
14. Torricella, F., Pierro, A., Mileo, E., Belle, V., and Bonucci, A. (2021). Nitroxide spin labels and EPR spectroscopy: A powerful association for protein dynamics studies. Biochim. Biophys. Acta, Proteins Proteomics *1869*, 140653. https://doi.org/10.1016/j.bbapap.2021.140653.
15. Jassoy, J.J., Berndhäuser, A., Duthie, F., Kühn, S.P., Hagelueken, G., and Schiemann, O. (2017). Versatile Trityl Spin Labels for Nanometer Distance Measurements on Biomolecules In Vitro and within Cells. Angew. Chem. Int. Ed. *56*, 177–181. https://doi.org/10.1002/anie.201609085.
16. Singewald, K., Hunter, H., Cunningham, T.F., Ruthstein, S., and Saxena, S. (2023). Measurement of Protein Dynamics from Site Directed Cu(II) Labeling. Analysis & Sensing *3*, e202200053. https://doi.org/10.1002/anse.202200053.
17. Banerjee, D., Yagi, H., Huber, T., Otting, G., and Goldfarb, D. (2012). Nanometer-Range Distance Measurement in a Protein Using Mn2+ Tags. J. Phys. Chem. Lett. *3*, 157–160. https://doi.org/10.1021/jz201521d.
18. Prokopiou, G., Lee, M.D., Collauto, A., Abdelkader, E.H., Bahrenberg, T., Feintuch, A., Ramirez-Cohen, M., Clayton, J., Swarbrick, J.D., Graham, B., et al. (2018). Small Gd(III) Tags for Gd(III)–Gd(III) Distance Measurements in Proteins by EPR Spectroscopy. Inorg. Chem. *57*, 5048–5059. https://doi.org/10.1021/acs.inorgchem.8b00133.
19. Lorenzi, M., Puppo, C., Lebrun, R., Lignon, S., Roubaud, V., Martinho, M., Mileo, E., Tordo, P., Marque, S.R.A., Gontero, B., et al. (2011). Tyrosine-targeted spin labeling and EPR spectroscopy: an alternative strategy for studying structural transitions in proteins. Angew. Chem., Int. Ed. Engl. *50*, 9108–9111. https://doi.org/10.1002/anie.201102539.
20. Mileo, E., Etienne, E., Martinho, M., Lebrun, R., Roubaud, V., Tordo, P., Gontero, B., Guigliarelli, B., Marque, S.R.A., and Belle, V. (2013). Enlarging the panoply of site-directed spin labeling electron paramagnetic resonance (SDSL-EPR): sensitive and selective spin-labeling of tyrosine using an isoindoline-based nitroxide. Bioconjugate Chem. *24*, 1110–1117. https://doi.org/10.1021/bc4000542.
21. Gmeiner, C., Klose, D., Mileo, E., Belle, V., Marque, S.R.A., Dorn, G., Allain, F.H.T., Guigliarelli, B., Jeschke, G., and Yulikov, M. (2017). Orthogonal Tyrosine and Cysteine Site-Directed Spin Labeling for Dipolar Pulse EPR Spectroscopy on Proteins. J. Phys. Chem. Lett. *8*, 4852–4857. https://doi.org/10.1021/acs.jpclett.7b02220.
22. Jeschke, G. (2018). The contribution of modern EPR to structural biology. Emerg. Top. Life Sci. *2*, 9–18. https://doi.org/10.1042/etls20170143.
23. Goldfarb, D. (2022). Exploring protein conformations in vitro and in cell with EPR distance measurements. Curr. Opin. Struct. Biol. *75*, 102398. https://doi.org/10.1016/j.sbi.2022.102398.
24. Bonucci, A., Ouari, O., Guigliarelli, B., Belle, V., and Mileo, E. (2020). In-Cell EPR: Progress towards Structural Studies Inside Cells. Chembiochem *21*, 451–460. https://doi.org/10.1002/cbic.201900291.
25. Theillet, F.-X. (2022). In-Cell Structural Biology by NMR: The Benefits of the Atomic Scale. Chem. Rev. *122*, 9497–9570. https://doi.org/10.1021/acs.chemrev.1c00937.
26. (2022). Goldfarb D. Exploring protein conformations in vitro and in cell with EPR distance measurements. Curr. Opin. Struct. Biol. *75*, 102398. https://doi.org/10.1016/j.sbi.2022.102398.
27. Fleck, N., Heubach, C.A., Hett, T., Haege, F.R., Bawol, P.P., Baltruschat, H., and Schiemann, O. (2020). SLIM: A short-linked, highly redox-stable trityl label for high sensitivity in cell EPR distance measurements. Angew. Chem. Int. Ed. *59*, 9767–9772. https://doi.org/10.1002/anie.202004452.
28. Galazzo L., Meier G., Januliene D., Parey K., De Vecchis D., Striednig B., Hilbi H., Schäfer L.V., Kuprov I., Moeller A., et al. The ABC transporter MsbA adopts the wide inward-open conformation in E. coli cells. Sci. Adv. 8:eabn6845. https://doi.org/10.1126/sciadv.abn6845.
29. Ketter S, Joseph B Gd(III) - trityl - nitroxide triple labelling and distance measurements in the heterooligomeric cobalamin transport complex in the native lipid bilayers. J. Am. Chem. Soc.,145 2:960–966. https://doi.org/10.1021/jacs.2c10080.
30. Nyenhuis, D.A., Nilaweera, T.D., Niblo, J.K., Nguyen, N.Q., DuBay, K.H., and Cafiso, D.S. (2020). Evidence for the Supramolecular Organization of a Bacterial Outer-Membrane Protein from In Vivo Pulse Electron Paramagnetic Resonance Spectroscopy. J. Am. Chem. Soc. *142*, 10715–10722.
31. Kucher, S., Korneev, S., Klare, J.P., Klose, Daniel, and Heinz-Jürgen, Steinhoff. (2020). «In cell Gd3+-based site-directed spin labeling and EPR spectroscopy of eGFP. Phys. Chem. Chem. Phys. *22*, 13358–13362. https://doi.org/10.1039/D0CP01930.
32. Pierro, A., Bonucci, A., Normanno, D., Ansaldi, M., Pilet, E., Ouari, O., Guigliarelli, B., Etienne, E., Gerbaud, G., Magalon, A., et al. (2022). Probing the Structural Dynamics of a Bacterial Chaperone in Its Native Environment by Nitroxide-Based EPR Spectroscopy. Chemistry *28*, e202202249. https://doi.org/10.1002/chem.202202249.
33. Karthikeyan, G., Bonucci, A., Casano, G., Gerbaud, G., Abel, S., Thomé, V., Kodjabachian, L., Magalon, A., Guigliarelli, B., Belle, V., et al. (2018). A Bioresistant Nitroxide Spin Label for In-Cell EPR Spectroscopy: In Vitro and In Oocytes Protein Structural Dynamics Studies. Angew. Chem. Int. Ed. *57*, 1366–1370. https://doi.org/10.1002/anie.201710184.
34. Martorana, A., Bellapadrona, G., Feintuch, A., Di Gregorio, E., Aime, S., and Goldfarb, D. (2014). Probing protein conformation in cells by EPR distance measurements using Gd3+ spin labeling. J. Am. Chem. Soc. *136*, 13458–13465. https://doi.org/10.1021/ja5079392.
35. Schmidt, M.J., Borbas, J., Drescher, M., and Summerer, D. (2014). A genetically encoded spin label for electron paramagnetic resonance distance measurements. J. Am. Chem. Soc. *136*, 1238–1241. https://doi.org/10.1021/ja411535q.

36. Schmidt, M.J., Fedoseev, A., Bücker, D., Borbas, J., Peter, C., Drescher, M., and Summerer, D. (2015). EPR Distance Measurements in Native Proteins with Genetically Encoded Spin Labels. ACS Chem. Biol. *10*, 2764–2771. https://doi.org/10.1021/acschembio.5b00512.
37. Torricella, F., Bonucci, A., Polykretis, P., Cencetti, F., and Banci, L. (2021). Rapid protein delivery to living cells for biomolecular investigation. Biochem. Biophys. Res. Commun. *570*, 82–88. https://doi.org/10.1016/j.bbrc.2021.07.006.
38. Torricella, F., Barbieri, L., Bazzurro, V., Diaspro, A., and Banci, L. (2022). Protein delivery to living cells by thermal stimulation for biophysical investigation. Sci. Rep. *12*, 17190. https://doi.org/10.1038/s41598-022-21103-9.
39. Pierro, A., Bonucci, A., Normanno, D., Ansaldi, M., Pilet, E., Ouari, O., Guigliarelli, B., Etienne, E., Gerbaud, G., Magalon, A., et al. Probing Structural Dynamics of a Bacterial Chaperone in Its Native Environment by Nitroxide-Based EPR Spectroscopy. Chemistry – A European Journal n/a. 10.1002/chem.202202249
40. Yang, Y., Yang, F., Gong, Y.-J., Bahrenberg, T., Feintuch, A., Su, X.-C., and Goldfarb, D. (2018). High Sensitivity In-Cell EPR Distance Measurements on Proteins using an Optimized Gd(III) Spin Label. J. Phys. Chem. Lett. *9*, 6119–6123. https://doi.org/10.1021/acs.jpclett.8b02663.
41. Pierro, A., and Drescher, M. (2023). Dance with spins: site-directed spin labeling coupled to electron paramagnetic resonance spectroscopy directly inside cells. Chem. Commun. *59*, 1274–1284. https://doi.org/10.1039/D2CC05907J.
42. Bellucci, M., Zambelli, B., Musiani, F., Turano, P., and Ciurli, S. (2009). Helicobacter pylori UreE, a urease accessory protein: specific Ni(2+)- and Zn(2+)-binding properties and interaction with its cognate UreG. Biochem. J. *422*, 91–100. https://doi.org/10.1042/bj20090434.
43. Etienne, E., Le Breton, N., Martinho, M., Mileo, E., and Belle, V. (2017). SimLabel: a graphical user interface to simulate continuous wave EPR spectra from site-directed spin labeling experiments. Magn. Reson. Chem. *55*, 714–719. https://doi.org/10.1002/mrc.4578.
44. Stoll, S., and Schweiger, A. (2006). EasySpin, a comprehensive software package for spectral simulation and analysis in EPR. J. Magn. Reson. *178*, 42–55. https://doi.org/10.1016/j.jmr.2005.08.013.
45. Mileo, E., Lorenzi, M., Erales, J., Lignon, S., Puppo, C., Le Breton, N., Etienne, E., Marque, S.R.A., Guigliarelli, B., Gontero, B., and Belle, V. (2013). Dynamics of the intrinsically disordered protein CP12 in its association with GAPDH in the green alga Chlamydomonas reinhardtii: a fuzzy complex. Mol. Biosyst. *9*, 2869–2876. https://doi.org/10.1039/c3mb70190e.
46. Zambelli, B., Musiani, F., Savini, M., Tucker, P., and Ciurli, S. (2007). Biochemical studies on Mycobacterium tuberculosis UreG and comparative modeling reveal structural and functional conservation among the bacterial UreG family. Biochemistry *46*, 3171–3182. https://doi.org/10.1021/bi6024676.
47. López, C.J., Fleissner, M.R., Guo, Z., Kusnetzow, A.K., and Hubbell, W.L. (2009). Osmolyte Perturbation Reveals Conformational Equilibria in Spin-Labeled Proteins*18* (Protein science : a publication of the Protein Society), pp. 1637–1652. https://doi.org/10.1002/pro.180.
48. Hubbell, W.L., López, C.J., Altenbach, C., and Yang, Z. (2013). Technological advances in site-directed spin labeling of proteins. Curr. Opin. Struct. Biol. *23*, 725–733. https://doi.org/10.1016/j.sbi.2013.06.008.
49. Flores Jiménez, R.H., Do Cao, M.A., Kim, M., and Cafiso, D.S. (2010). Osmolytes modulate conformational exchange in solvent-exposed regions of membrane proteins. Protein Sci. *19*, 269–278. https://doi.org/10.1002/pro.305.
50. Jagtap, A.P., Krstic, I., Kunjir, N.C., Hänsel, R., Prisner, T.F., and Sigurdsson, S.T. (2015). Sterically shielded spin labels for in-cell EPR spectroscopy: analysis of stability in reducing environment. Free Radic. Res. *49*, 78–85. https://doi.org/10.3109/10715762.2014.979409.
51. Speer, S.L., Stewart, C.J., Sapir, L., Harries, D., and Pielak, G.J. (2022). Macromolecular Crowding Is More than Hard-Core Repulsions. Annu. Rev. Biophys. *51*, 267–300. https://doi.org/10.1146/annurev-biophys-091321-071829.
52. Sharp, K.A. (2016). Unpacking the origins of in-cell crowding. Proc. Natl. Acad. Sci. USA *113*, 1684–1685. https://doi.org/10.1073/pnas.1600098113.
53. Akabayov, B., Akabayov, S.R., Lee, S.-J., Wagner, G., and Richardson, C.C. (2013). Impact of macromolecular crowding on DNA replication. Nat. Commun. *4*, 1615. https://doi.org/10.1038/ncomms2620.
54. Stagg, L., Zhang, S.-Q., Cheung, M.S., and Wittung-Stafshede, P. (2007). Molecular crowding enhances native structure and stability of α/β protein flavodoxin. Proc. Natl. Acad. Sci. USA *104*, 18976–18981. https://doi.org/10.1073/pnas.0705127104.
55. Zhou, B.R., Zhou, Z., Hu, Q.L., Chen, J., and Liang, Y. (2008). Mixed macromolecular crowding inhibits amyloid formation of hen egg white lysozyme. Biochim. Biophys. Acta *1784*, 472–480. https://doi.org/10.1016/j.bbapap.2008.01.004.
56. Street, T.O., Bolen, D.W., and Rose, G.D. (2006). A molecular mechanism for osmolyte-induced protein stability. Proc. Natl. Acad. Sci. USA *103*, 13997–14002. https://doi.org/10.1073/pnas.0606236103.
57. Parray, Z.A., Hassan, M.I., Ahmad, F., and Islam, A. (2020). Amphiphilic nature of polyethylene glycols and their role in medical research. Polym. Test. *82*, 106316. https://doi.org/10.1016/j.polymertesting.2019.106316.
58. Jeschke, G. (2018). MMM: A toolbox for integrative structure modeling. Protein Sci. *27*, 76–85. https://doi.org/10.1002/pro.3269.
59. Schiemann, O., Heubach, C.A., Abdullin, D., Ackermann, K., Azarkh, M., Bagryanskaya, E.G., Drescher, M., Endeward, B., Freed, J.H., Galazzo, L., et al. (2021). Benchmark Test and Guidelines for DEER/PELDOR Experiments on Nitroxide-Labeled Biomolecules. J. Am. Chem. Soc. *143*, 17875–17890. https://doi.org/10.1021/jacs.1c07371.
60. Kucher, S., Elsner, C., Safonova, M., Maffini, S., and Bordignon, E. (2021). In-Cell Double Electron–Electron Resonance at Nanomolar Protein Concentrations. J. Phys. Chem. Lett. *12*, 3679–3684. https://doi.org/10.1021/acs.jpclett.1c00048.
61. Joseph, B., Sikora, A., and Cafiso, D.S. (2016). Ligand Induced Conformational Changes of a Membrane Transporter in E. coli Cells Observed with DEER/PELDOR. J. Am. Chem. Soc. *138*, 1844–1847. https://doi.org/10.1021/jacs.5b13382.
62. Fábregas Ibáñez, L., Jeschke, G., and Stoll, S. (2020). DeerLab: a comprehensive software package for analyzing dipolar electron paramagnetic resonance spectroscopy data. Magnes. Res. *1*, 209–224. https://doi.org/10.5194/mr-1-209-2020.

STAR★METHODS

KEY RESSOURCES TABLE

REAGENT or RESOURCE	SOURCE	IDENTIFIER
Antibodies		
We don't used them in this study.		
Bacterial and virus strains		
Escherichia coli BL21-DE3 competent cells	New England Bio Labs	C2527H
Escherichia coli NEB® 5-alpha competent cells	New England Bio Labs	C2987H
Biological samples		
We don't used them in this study.		
Chemicals, peptides, and recombinant proteins		
3-Maleimido-PROXYL	Sigma-Aldrich	253375; CAS: 5389-27-5
Deuterated glycerol (Glycerol d8)	Sigma-Aldrich	447498; CAS: 7325-17-9
Recombinant DNA		
Plasmid: pET3a-SpureG	Zambelli et al. *J Biol Chem*. 2005 Feb 11; 280(6):4684-95. https://doi.org/10.1074/jbc.M408483200.	
Plasmid: pET22b-sfGFP	Gen Script	
Plasmid: pET3a-SpureG G9C D158C	Gen Script	
Plasmid: pET3a-SpureG G9C	Gen Script	
Plasmid: pET3a-SpureG D158C	Gen Script	
Software and algorithms		
Napari (0.4.16) viewer and MiSiC plugin		https://pypi.org/project/misic-napari/ and https://napari.org/stable/
Fiji 1.53s		https://imagej.nih.gov/ij/index.html
SimLabel	E. Etienne et al. *Molecules* 2023, *28*(3), 1348.	https://easyspin.org/forum/viewtopic.php?f=8&t=297
DeerLab	Fábregas Ibáñez, L. et al. *Magn. Reson.*, 2020, 1, 209–224	https://jeschkelab.github.io/DeerLab/
DEERNet	Worswick, S. G. et al. *Sci. Adv.* 2018,4, eaat5218.	The source code of DEERNet and its descrambler routines are available as a part of the open-source Spinach package (spindynamics.org)
Extract_from2D		https://bip.cnrs.fr/epr-facility/software-and-scripts/
Kinetic_intensity		https://bip.cnrs.fr/epr-facility/software-and-scripts/

RESOURCE AVAILABILITY

Lead contact

Further information and requests for resources and reagents should be directed to and will be fulfilled by the lead contact, Elisabetta Mileo (emileo@imm.cnrs.fr)

Materials availability

The plasmids generated in this study are available from the lead contact on reasonable request.

Data and code availability

- Data: All the data reported in this study are available from the lead contact on reasonable request.
- Code: Information about the two in-house developed MATLAB scripts (extract_from2D and kinetic_intensity) can be found following the links indicated in the key resources table.

- Other items: Any additional information required to reanalyze the data reported in this paper is available from the lead contact upon request.

METHODS DETAILS

*Sp*UreG purification and spin-labeling

*Sp*UreG-WT and its variants are cloned in a pET-3a vector and transformed in an *E. coli* BL21-DE3 strain. As previously reported, cells are coltured in LB medium until reaching OD600 = 0.6 and induced by 0.5 mM IPTG for 18 h at 20°C.[10] Cells are harvested by centrifugation at 5000 rpm 20 min at 4°C and resuspended in 60mL of 50mM Tris-HCl pH 8, containing 5mM EDTA, 2mM DTT, 10mM $MgCl_2$ and 20 μg/ml DNase I. Cells are lysed by French pressure cell homogenizer (Stansted Fluid Power LTD) at 15000 pounds/square inch, and the supernatant is separated by centrifugation at 14000 rpm 30 min at 4°C. The protein purification is tag-less and involves an Anion Exchange Column previously equilibrated against 20 mM Tris-HCl pH 8 buffer containing EDTA 5 mM, 2mM DTT (AEC, Q-Sepharose 26/10, GE Healthcare). This step is followed by two Size Exclusion Chromatography columns (HiLoad Superdex XK 75 16/60 column and Superdex XK 75 13/300, GE Healthcare) against 20 mM Tris-HCl pH 8 buffer, containing NaCl 150 mM and TCEP (tris(2-carboxyethyl) phosphine) 1 mM. Prior to spin-labeling, TCEP is removed from 100 nmols of protein by PD10 desalting column (GE Healthcare) against Tris-HCl 10 mM pH7.4 buffer. The fractions containing the protein are pooled and incubated with maleimido-proxyl nitroxide (Sigma-Aldrich) in 10-fold molar excess/cysteine. A second PD10 desalting column against the same buffer described above is performed to remove the unbound spin-label's excess. The collected fractions are then checked by EPR spectroscopy and polished by centrifugation in 2 mL Vivaspin concentrators 3kDa MWCO. The concentration of the labeled protein is evaluated by measuring the OD at 280 nm. The labeling yield (over 90%) was calculated by comparing the spin concentration (obtained by EPR spectroscopy) with the protein concentration.

*sf*GFP purification

*sf*GFP encoded in a pET22b vector tagged with a-6His tail is overexpressed in *E. coli* BL21-DE3 strain. The cells are grown in LB medium at 37°C until reaching OD600 = 0.4. The overexpression is induced by addition of 0.4 mM of IPTG and growth for 4 h at 37°C. Cells are harvested by centrifugation at 4500 rpm 20 min at 4°C and resuspended in Tris-HCl 20mM pH 7.4 buffer, containing NaCl 150mM and protease inhibitors EDTA-free cocktail (Roche). After three passages into EmulsiFlex (Avestin) at 1500 psi, the supernatant is separated by centrifugation at 45000 rpm for 50 min.

The supernatant is loaded in a Ni-NTA superflow column 5 mL (Qiagen) equilibrated with Tris-HCl 20 mM pH 7.4, NaCl 150 mM, Imidazole 10 mM sfGFP elutes in Tris-HCl 20 mM pH 7.4, NaCl 150 mM, Imidazole 200 mM. Fractions containing the protein are then dialyzed in a 3 kDa MWCO membrane against 500 mL Tris-HCl 20 mM pH 7.4, NaCl 150 mM for 2 h, renovating the buffer every 30 min. Protein concentration was estimated using absorbance at 485 nm and an extinction coefficient ε400 = 83300 M-1cm-1 (http://us.expasy.org/cgi-bin/protparam).

Preparation of competent *E. coli* cells for heat-shock

An overnight pre-culture of *E. coli* NEB 5-alpha cells is diluted to a final *OD*600 = 0.05 into 20 mL of LB medium and cultured at 37°C until reaching OD_{600} = 0.6. The growth is, then, stopped by chilling the cells at 4°C on ice for at least 30 min. Bacterial cells are harvested by centrifugation at 4000 *x g* at 4°C for 15 min and re-suspended in 10 mL of sterile CaCl2 50 mM. This mixture is incubated for 2 h at 4°C. Finally, bacterial cells are harvested 3800 *x g* 10 min at 4°C and resuspended in $CaCl_2$ 10 mM to obtain a final concentration between 4 and 7 * 10^{10} *cells/mL*. Cells are incubated at 4°C for at least 20 min and used for an in-cell EPR experiment in the same day.

Preparation of competent *E. coli* cells for electroporation

Electrocompetent cells were prepared as previously reported.[39] An overnight pre-culture of *E. coli* NEB 5-alpha cells is inoculated in 100 mL LB medium to a final *OD*600 = 0.05 and incubated at 37°C until reaching *OD*600 = 0.9. After chilling the cells at 4°C on ice for at least 30 min, they are harvested by centrifugation at 4000 *x g* for 10 min at 4°C and re-suspended in 100mL of sterile MilliQ water +10% glycerol. This step is repeated two times, reducing the volume of the washes to 60 mL and 50 mL, respectively. Finally, bacterial cells are resuspended in sterile MilliQ water +10% glycerol. The cell number was estimated between 4 and 7 * 10^{10}*cells/mL*. Cells can be aliquoted and stored at −80°C.

Protein delivery by heat-shock and electroporation

As first step, 20 μL of competent cells are incubated with 20 μL of labeled protein 10 min on ice. For electroporation, the protein must be without salt to avoid arching. For electroporation, teh protein-cells mixture is, then, transferred into a pre-chilled 1 mm-gap cuvette (VRW) and electroporated in a Gene Pulser Xcell from Bio-Rad, using the following parameters: 1800 V/cm, 200 Ω, 25μF, 1 msec pulse. For heat shock, the mixture is incubated 2 min at 42°C and 2 min at 4°C. In both protocols, the cells membrane integrity is recovered by addition of 500 μL of pre-warmed SOC.

Cells are then washed by centrifugation at 3200 *x g*, 2 min at 4°C three times: 500μL of PBS (Phosphate Buffer 10 mM pH 7.5, KCl 2.7 mM, NaCl 137 mM) + 0.005% Triton solution, in the first wash, 500 μL of PBS until the excess of not internalized protein is completely removed

(4 washes for heatshock and 3 washes for electroporation). For CW-EPR at room temperature the pellet is resuspended in 50 μL of PBS with 1% LT-Agarose (Euromedex) and transferred in an EPR quartz capillary. For confocal microscopy 4 μL of sample are transferred on an agar pad.

Fluorescence Microscopy

Imaging was performed using an inverted fluorescence confocal microscope, Olympus FV1000-IX81 with an 100X/1.40 objective oil immersion. Images were acquired using a laser excitation at 488nm and emission fluorescence was recovered in the range 500-600nm. The transmission image is also recovered in order to determine the outline of the bacteria.

Fluorescence microscopy image analysis

The transmission images were first segmented using the Napari (0.4.16) viewer and the MiSiC plugin https://pypi.org/project/misic-napari/, in order to detect each bacterium individually. Then the fluorescence was measured using Fiji (1.53s) for each bacterium and divided by the average fluorescence of the image background, to obtain a signal to noise ratio. The ratios were sorted in ascending order and plotted in a graph for the conditions tested (heat shock of sfGFP and *E. coli* cells in $CaCl_2$ 50mM or $CaCl_2$ 10mM and *E. coli* cells in $CaCl_2$ 10mM in contact with sfGFP).

CW-EPR experiments *in vitro* and in crowded solutions

All the room temperature CW-EPR experiments are recorded at room temperature on a spectrometer Elexsys 500 (Bruker) equipped with a Super High Q sensitivity resonator at X band (9.9GHz). Samples are injected in a quartz capillary whose sensible volume was 40μL and recorded using the following parameters: microwaves power = 10mW; magnetic field modulation amplitude = 1G; field sweep = 150G; receiver gain = 60dB. Simulations of CW-EPR spectra, performed using SimLabel,[43] a GUI of EasySpin,[44] are detailed in the Supplemental Information, from Figures S11–S29.

In crowding experiments, crowding agents are dissolved in 10 mL of 10 mM Tris buffer pH 7.4 to obtain the desired concentration. To do not dilute the solution, 5 μL of protein are added to this solution to obtain a final concentration of 50 μM in 50 μL.

The reduction profiles presented in Figure 5 result from 2D experiments (field sweep and time): for field sweep EPR spectra acquisition we used the same parameters described before in this section, while the delay between the acquisition of each spectrum was of 90 s.

DEER experiments

For *in vitro* studies, *Sp*UreG_C68A-G9C^{proxyl}/D158C^{proxyl} was diluted in a buffer containing 30% of glycerol, as a cryoprotector. Concerning in-cell EPR samples, after the delivery of the protein inside the cell by heat-shock or electroporation, the excess of not internalized protein is removed by washing the pellet with deuterated PBS four times as described for CW-EPR samples. Cells are then resuspended in deuterated PBS enriched with 30% of glycerol D8, transferred in a quartz Q-band capillary and flash-frozen in liquid nitrogen. The time between the delivery trigger and the freezing was between 12 and 15 min. DEER distance measurements were performed at 60K on a Bruker ELEXSYS E580 spectrometer equipped with an Oxford helium temperature regulation unit at Q-band using the standard EN 5107D2 resonator. All the measurements were performed at 60K on 20 μL of sample. The DEER traces were, then, analyzed using DeerLab software.[62] as recommended in literature[59] (https://github.com/JeschkeLab/DeerLab, ETH, Zürich, Switzerland).

QUANTIFICATION AND STATISTICAL ANALYSIS

Data showed in Figure 5 were analyzed using in-house developed MATLAB scripts, "extract_from2D" and "kinetic_intensity".

Extract_from2D was used to sum ten consecutive spectra of the 2D EPR experiments (normally caracterized by between 500 and 700 spectra) in order to obtain a 2D experiment having ten times less spectra but a higher signal to noise ratio.This home-made MATLAB software uses some EasySpin functions[44] (extract_from2D, mode 2D/group spectra, available here: https://bip.cnrs.fr/epr-facility/software-and-scripts/). Spectra treated with extract_from2D were then analyzed using kinetic_intensity, a MATLAB home made software using some EasySpin functions[44] (available here: https://bip.cnrs.fr/epr-facility/software-and-scripts/). This script enables: *i*) to plot the absorption spectrum (numerically obtained) of each experimental spectra of a 2D experiment, *ii*) to apply a baseline correction, managed by the user, on the absorption spectra, *iii*) to automatically extract the numerical integrated intensity of the corrected spectra and *iv*) to plot the obtained intensities versus the time of the spectra aquisition (automatically extracted).